Direct numerical simulation of thermal channel flow for medium–high Prandtl numbers up to $Re_\tau = 2000$

F. Alcántara-Ávila, S. Hoyas*

Instituto Universitario de Matemática Pura y Aplicada, Universitat Politècnica de València, Valencia 46022, Spain

ARTICLE INFO

ABSTRACT

A new set of DNS of a thermal channel flow have been conducted for friction Reynolds and Prandtl numbers up to 2000 and 10, respectively, reaching the Prandtl number of water, 7, for new Reynolds numbers, never simulated before. The Mixed Boundary Condition has been used as the thermal boundary condition. A new scaling of the thickness of the conductive sublayer is presented for medium–high Prandtl number values. The maximum of the intensity of the thermal field does not increase with the Reynolds number for the highest Prandtl numbers. This entails a good scaling near the wall of the viscous diffusion and the dissipation terms in the budgets of the temperature variance. The Nusselt number shows a power function behaviour with respect to the Prandtl number in a certain range of the friction Péclet number. Finally, the turbulent Prandtl number presents an increase near the wall for highest Prandtl numbers due to the reduction of the thermal eddy diffusivity. The statistics of all simulations can be downloaded from the web page of our group: http://personales.upv.es/serhocal/.

1. Introduction

In the last decades, the use of Direct Numerical Simulations (DNS) of turbulent flows has become a main tool to understand the behaviours of the flow. The emergence of the DNS occurred in 1987 with the work of Kim et al. [1] for a turbulent channel flow. Due to the high computational cost of this kind of simulations, only canonical geometries can be studied, such as boundary layers, pipes or channel flows. The latter one is the aim of study of this work.

Introducing the energy equation into the simulation requires extra computational power, specially if the thermal channel flow is very turbulent, i.e. the Prandtl number is high. The first DNS of a thermal channel flow was performed by Kim and Moin [2]. A friction Reynolds number $Re_\tau = u_\tau h/\nu = 180$ and Prandtl numbers of values $Pr = 0.1$, 0.7 and 2 were used. Here, $u_\tau = \sqrt{\tau_w/\rho}$ is the friction velocity, h is the semi height of the channel and ν is the kinematic viscosity. In the definition of the friction temperature, τ_w is the shear stress at the wall and ρ is the density of the fluid. The boundary condition for the thermal field in [2] was an internal heat generation in the center of the channel. Since then, the aim has been to increase the Reynolds number and/or to study a wider range of Prandtl numbers [3–12].

In the work done by Kasagi et al. [4], the Mixed Boundary Condition (MBC) was introduced for the first time in a DNS. For this boundary condition, both walls are heated with an averaged constant uniform heat flux, and the average temperature of the walls is independent of time and increases linearly in the streamwise direction. The MBC is the thermal condition used in this work. Later, Kawamura et al. [5] performed the first simulation of a thermal flows with Prandtl numbers up to a value of 5, for $Re_\tau = 180$. They modelled the velocity and thermal fluctuations near the wall as expansion in terms of the inner coordinate y^+, finding that the coefficients were mostly independent of Pr for $Pr > 0.2$. Also in the same line of work, Na et al. [6] and Seki et al. [13] performed a new set of simulations, using $Re_\tau = 150$ and 180, respectively, for Prandtl number values up to 10. Among other things, they found an increase of Pr_t near the wall for $Pr \geq 3$. The reason of this increase in Pr_t was a decrease of the turbulent diffusivity for these medium–high Prandtl numbers. Also, Na et al. [6] computed the thickness of the conductive sublayer, Δ_θ, obtaining that it varies as $Pr^{-1/2}$ in the range of Prandtl between 1 to 10. Another set of DNS performed by Schwertfirm and Manhart [14], up to $Pr = 50$ for $Re_\tau = 180$, show a continuation of the results from the previous works cited.

---

* Corresponding author.
  E-mail address: serhocal@mot.upv.es (S. Hoyas).

Regarding the Reynolds number dependencies, it has always been challenging to increase the Re_τ simulated due to the increase of computational power required. Yano and Kasagi [15] stated that the computational cost can be approximated as $L_x^2 L_y Re_\tau^4 Pr^{3/2}$. Kawamura et al. [16] increased the Reynolds number simulated up to $Re_\tau = 395$, using the same boundary condition that in [4], i.e. the MBC. First order statistics and the budget terms of turbulent heat fluxes and the temperature variance were calculated. Also, images of the instantaneous velocity and thermal fields were obtained to analyse the similarities and differences of the structures of each field. Finally, a weak effect of the Reynolds number was observed in the turbulent Prandtl number, Pr_t. A few years later, Abe et al. [8] reached Reynolds numbers of $Re_\tau = 640$ and 1020 for a regular Prandtl number of 0.71 and a low Prandtl number of 0.025. They found that the temperature fluctuations increased with the Reynolds number, specially for the low Prandtl number case, because of the increasing convective effect. Using the same database, Abe and Antonia [17] analyse the temperature field comparing it with the velocity one, by means of temperature gradients and vorticity. They found high correlations between both fields when the Prandtl number was close to 1, specially in the near wall region, and this correlation was mainly independent of the Reynolds number. They also focused on the production terms of the transport equation of the temperature dissipation. It was obtained that, for those Reynolds and Prandtl numbers, only the gradient production term was independent of the Reynolds number. Finally, it is worth to mention the work done by Pirozzoli at al. [10], where the highest Reynolds number for a thermal channel flow was simulated, $Re_\tau = 4000$. In this simulation, a first hint of the emergence of a logarithmic layer was observed.

In this work, we have simulated friction Reynolds numbers of values 500, 1000 and 2000, increasing the Prandtl number up to values of 10, 7 and 7, respectively. We try to assess the Reynolds number effect and especially, the Prandtl number effects, on several flow statistics. In the next section, the flow problem set up and the numerical procedure used are presented. The third section contains the results obtained. The fourth and last section contains the conclusion.

2. Methodology

In this work, several DNS of a passive thermal flow in a Poiseuille turbulent channel are presented. The flow is considered incompressible and the MBC is used. The domain of every simulation is a computational box of dimensions $2\pi h \times 2h \times \pi h$ in the streamwise (x), wall-normal (y) and spanwise (z) directions, respectively, with corresponding velocities U, V and W. According to Lozano-Durán and Jiménez [18] and Lluesma-Rodríguez et al. 2018 [11], these dimensions of the computational box are large enough to properly calculate the first-order turbulent statistics of the velocity and temperature field, respectively. Temperature is denoted by T and the transformed temperature (defined below), by Θ. Reynolds decomposition is used, and the variables (uppercase) are divided in mean (uppercase and overbar) and fluctuating (lowercase) parts, i.e. $U = \overline{U} + u$. The superscript $^+$ indicates normalization in wall units: u_τ, θ_τ and ν, where $\theta_\tau = q_w/(\rho c_p u_\tau)$ is the friction temperature, and q_w is the heat flux at the wall, while c_p is the specific heat at constant pressure.

The Navier-Stokes and the energy equations are used to simulate the flow

$$\partial_j U_j^+ = 0, \tag{1a}$$

$$\partial_t U_i^+ + U_j^+ \partial_j U_i^+ = -\partial_i P^+ + \frac{1}{Re_\tau} \partial_{jj} U_i^+, \tag{1b}$$

$$\partial_t \Theta^+ + U_j^+ \partial_j \Theta^+ = \frac{1}{Re_\tau Pr} \partial_{jj} \Theta^+ + U^+ / \langle U^+ \rangle_{xyz}. \tag{1c}$$

Here, $\langle \rangle_{xyz}$ denotes averaging in the three dimensions and time. Therefore, $\langle U^+ \rangle_{xyz} = U_b^+$, i.e. the bulk velocity. The code used to run the simulations is the LISO code, already validated in several different turbulent flows, [11,19–23]. Periodicity in the streamwise and spanwise dimensions allows the use of high efficient Fourier methods in these directions. In order to make the temperature, T, periodic, the linear increase of temperature in the streamwise direction due to the use of the MBC must be subtracted. The transformed temperature, Θ is used to achieve this. It is defined as $\Theta = T_w - T$, where T_w is the temperature at the wall that carries the non-periodic part of T. In order to solve Eqs. (1a)-(1c), the same method than in Lluesma et al. [11] has been employed. This method is based on the one used by Kim et al. [1], where the Navier Stokes equations are transformed into equations for the wall-normal vorticity, Ω_t, and the Laplacian of the wall-normal velocity, Φ. The rest of the variables can be recovered from these two by using the continuity and vorticity equations. The discretization methods are dealiased Fourier expansions in the x and z directions. In the y direction, a seven-point compact finite differences scheme with fourth-order consistency and extended spectral-like resolution is used [24]. For the temporal discretization, a third-order semi-implicit Runge-Kutta scheme has been implemented. [25].

Table 1 presents the most important parameters of the simulations. Left subtable shows the dimensionless numbers of all the simulations that have been conducted for this work. Mesh resolution and time of each simulation in wash-outs is also shown. A wash-out is defined as the time needed for an eddy to cross the channel, L_x/U_b, where L_x is the dimension of the box in the streamwise direction. Δy_w^+ and Δy_{cl}^+ are the wall-normal mesh resolution in the wall and in the center line of the channel, respectively. The mesh resolution in the wall-normal direction is adapted to satisfy Batchelor length scale, $\eta_\theta = \eta Pr^{-1/2}$, where η is the local isotropic Kolmogorov scale $\eta = (\nu^3/\epsilon)^{1/4}$. Note that since $Pr \geq 1$ for all cases, the Batchelor length scale will always be the restricting scale to set the mesh resolution. Meanwhile, the mesh resolution in the developed directions for medium Prandtl number is similar to many other trusted simulations [5,8,26]. The mesh resolution in x and z directions has also been adapted for higher Prandtl numbers. In addition, for medium–high Prandtl numbers a mesh with higher resolution in x and z and/or y was simulated for testing. There were not significant differences in the first order statistics between the different meshes simulated. The right subtable in Table 1 shows the symbols, colours and line styles to distinguish each simulations throughout all the plots of this paper (unless otherwise specified). The data for Prandtl numbers below 1 is taken from Alcántara et al. [12]. Values of cases with Prandtl numbers of 0.5, 0.1, 0.02 and 0.01 are also used in plots where the Prandtl number is the variable.

A good way to observe the size of the turbulent scales is by plotting isocontours of velocity and temperature fields. They can be seen in Fig. 1, where different instantaneous values of the velocity and temperature field are presented. In Fig. 1a and b, a comparison between both fields, velocity and temperature for $Re_\tau = 2000$ and $Pr = 7$, is done in a $x - y$ plane. Unlike temperature fields for $Pr = 1$, where the temperature scales are similar to the ones of the velocity field, as presented in [12], the temperature scales for $Pr = 7$ are smaller than the velocity ones. This implies that the temperature field is more turbulent than the velocity one, and, effectively, a finer mesh is needed to properly capture the smaller scales of the thermal field. In addition, one can easily see how the boundary layer of the temperature is thinner than the one of the velocity, what implies higher gradients of temperature in the near-wall region. Remark the fact that both, velocity and temperature structures detach from the wall with an angle of approximately 25°.

Table 1
Parameters of the simulations. On the left subtable, dimensionless numbers are indicated together with the mesh resolution and the time of the simulation in wash-outs. On the right subtable it is shown the symbols, colours and line styles to refer to each simulation in the plots through all the paper, unless otherwise specified.

| Re_τ	Pr	Re	Δx^+	Δz^+	Δy_w^+	Δy_{cl}^+	W.O.	Pr	Symbol	Re_τ 500	1000	2000
500	1	10200	8.18	4.09	0.72	5.3	143	10	*	▬	▬	▬
500	2	10200	8.18	4.09	0.72	5.3	191	7	△			
500	4	10200	8.18	4.09	0.72	5.3	288	4	○			
500	7	10200	8.18	4.09	0.27	3.9	94	2	□			
500	10	10200	4.09	2.05	0.22	3.6	120	1	▽			
1000	1	22300	8.18	4.09	0.44	7.4	191	0.71	○	▬ ▬	▬ ▬	▬ ▬
1000	2	22300	8.18	4.09	0.44	7.4	119	0.3	△			
1000	4	22300	8.18	4.09	0.19	4.9	185	0.05	▷			
1000	7	22300	4.09	2.05	0.16	4.5	86	0.007	▽			
2000	1	48500	8.18	4.09	0.32	8.8	97					
2000	2	48500	8.18	4.09	0.32	8.8	96					
2000	4	48500	8.18	4.09	0.12	4.3	56					
2000	7	48500	4.09	2.05	0.12	4.3	27					
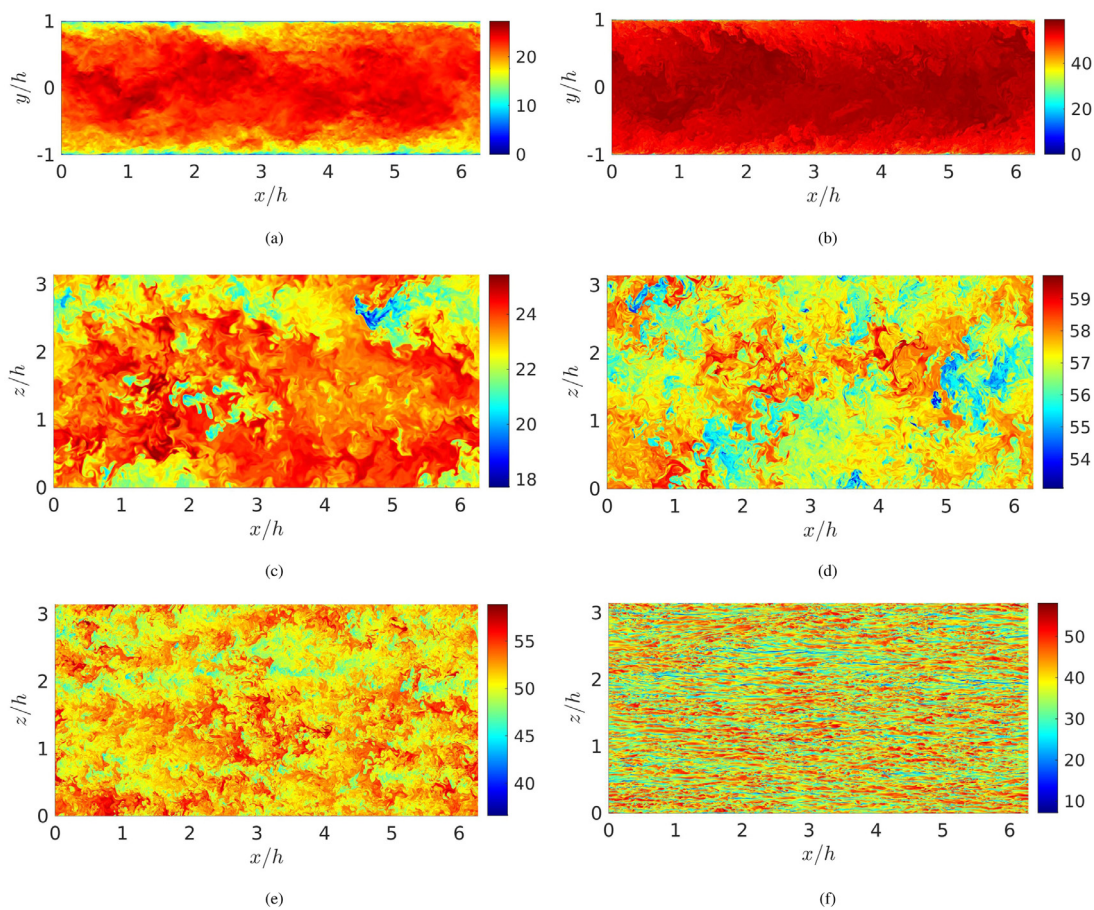
Fig. 1. Instantaneous images for $Re_\tau = 2000$. (a) Velocity and (b) temperature fields for the $Pr = 7$ case in the $x - y$ plane. Temperature field for (c) $Pr = 1$ and (d) $Pr = 7$ in the $x - z$ central plane of the channel. Temperature field for $Pr = 7$ in a $x - z$ plane located in (e) the logarithmic region, $y^+ = 240$, and (f) in the near-wall region, $y^+ = 9$. All magnitudes are normalized in wall units.

The middle Fig. 1c and d, present the temperature field in a $x - z$ plane located in the center of the channel for the cases of $Pr = 1$ and 7, respectively, with $Re_\tau = 2000$. Following the same idea as before, smaller turbulent scales appear for $Pr = 7$. Finally, a comparison of the temperature scales has been done, depending on the distance to the wall. Fig. 1e and f are instantaneous images of the temperature field for $Pr = 7$ and $Re_\tau = 2000$ at $y^+ = 240$ and 9, respectively, i.e. the logarithmic and the near-wall region. In the logarithmic region, intermediate scales are obtained, not as big as in the outer region, but either as small as in the near-wall region.

The classical streaks in the near wall region are perfectly observed in Fig. 1f. Corresponding streaks for the velocity field are also obtained (not shown here for brevity), which reflect the strong correlations between the streamwise velocity and temperature field in the near-wall region. However, it should be noted that this correlation get weaker as the Prandtl number increases, as it will be shown later.

For the first time, simulation with Reynolds number of values 500–2000 have been performed for Prandtl number values from 1 to 10. Table 2 presents which simulations were already performed

Table 2

Former and new simulations. □: Na et al. [6]; △: Seki et al. [13]; ⊙: Schwertfirm and Manhart [14]; ×: Kozuka et al. [9]; + : New simulations from this work.

Pr–Re_τ	150–180	395	500	1000	2000
1	□ △	×	+	+	+
2	△	×	+	+	+
3	□ ⊙				
4			+	+	+
5		×			
7		×	+	+	+
10	□ △ ⊙	×	+		
25	⊙				
50	⊙				

and the new contributions from this work. All the simulations from this work are new in terms of the Re_τ and Pr combinations, allowing a wider view of the physical behaviour of the thermal field in turbulent channels.

In order to run the simulation, an initial file from other simulation with similar Reynolds and Prandtl numbers is used. The process when the flow converges towards a statistically stationary state can be almost as long as the simulation itself. After that, the simulation is run for the time stated in Table 1, and the flow statistics are collected. Approximately 20 wash-outs are needed for the highest Reynolds numbers simulations. After this point, in order to check if the flow statistics are converged, the balance equations of the momentum and energy equations are computed. These balance equations are obtained by integration of Eqs. (1a)–(1c).

$$\tau_{total}^+ = \overbrace{\underbrace{\frac{1}{Re_\tau}\frac{d\overline{U}^+}{dy}}_{\text{Molecular}} \ \overbrace{-\overline{uv}^+}^{\text{Turbulent}}}^{} = \overbrace{1 - \frac{y}{h}}^{\text{Total}},$$
(2a)

$$q_{total}^+ = \underbrace{\frac{1}{Re_\tau Pr}\frac{d\overline{\Theta}^+}{dy}}_{\text{Molecular}} \ \underbrace{-\overline{v^+\theta^+}}_{\text{Turbulent}} = \underbrace{1 - \frac{1}{Re_\tau}\int_0^{y^+}\frac{\overline{U}_1^+}{\langle U^+\rangle_{xyz}}\,dy}_{\text{Total}}.$$
(2b)

When the balances in shear stresses and heat fluxes are below 10^{-3} the simulation is considered converged. Fig. 2a for the velocity and 2b for the temperature show the balances terms of Eqs. (2a) and (2b). Red dotted line is the residual of the LHS and RHS of Eqs. (2a) and (2b), which indicates that the simulations are converged. Similar plots are obtained for $Re_\tau = 500$ and 1000, but they are not shown here for brevity.
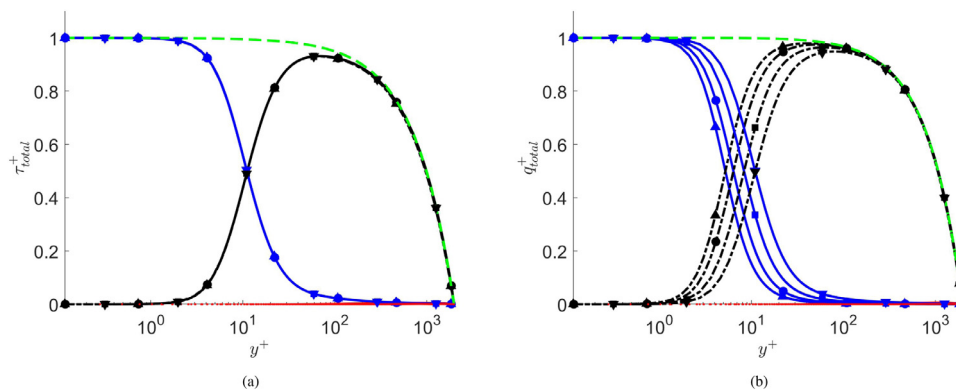
3. Results

3.1. Temperature statistics

The mean temperature, $\overline{\Theta}^+$, is presented in Fig. 3a as $\overline{\Theta}^+/Pr$. The law of the wall, $\overline{\Theta}^+ = Pr \cdot y^+$, is fulfilled for every flow close to the wall. The size of this region of the flow, Δ_θ, called conductive sublayer, is defined by the value of the y^+ coordinate where $\overline{\Theta}^+$ differs by a 5% with the law of the wall.

As its name indicates, in this region the heat transferred by conduction is dominant over the turbulent heat flux. It can be seen how this layer gets thinner as the Prandtl number increases. In Fig. 3b it is represented Δ_θ for every case. Due to the discretization of the problem, there is noise in the value of Δ_θ, specially when its value is low, see dashed lines of Fig. 3b. A linear interpolation of $\overline{\Theta}^+/Pr$ between the two closest mesh points where $\overline{\Theta}^+$ differs by a 5% with the law of the wall gives a more realistic result of where Δ_θ is actually located (solid lines of Fig. 3b). The depth of the conductive sublayer ranges from values of 100 for very low Prandtl numbers down to barely 3 wall units for $Pr = 7$ and 10. This is a great indicator that for low Prandtl numbers, the thermal field is dominated by conductive heat transfer, and as the Prandtl increases, the turbulent heat transfer overcomes the conductive one.

The classical scaling proposed for Δ_θ is a power function, such as $\Delta_\theta \sim Pr^{-0.5}$, $\Delta_\theta \sim Pr^{-1/3}$, $\Delta_\theta \sim Pr^{-0.3}$ or $\Delta_\theta \sim Pr^{-0.29}$, depending on the range of Prandtl numbers, [6,14,27,28], respectively. A more precise way to define the scaling of Δ_θ is using a power function with a dependence on the Prandtl number in the exponent, $\Delta_\theta \sim Pr^\gamma$, where $\gamma = \gamma(Pr)$. Thus, the following relation can be used $\Delta_\theta = aPr^\gamma$, where a must be the value of Δ_θ for $Pr = 1$. Then, the value of γ for every other Prandtl numbers is calculated as $\gamma = \ln(\Delta\theta/a)/\ln(Pr)$ to fit the data. Note that, for the value of γ at $Pr = 1$ an indeterminate form of the type 0/0 is obtained. Therefore, limits must be used to obtain this specific value. As can be seen in Fig. 3b, the value of γ is a linear function of Pr for $Pr \geq 0.5$ (x-axis is in logarithmic scale). Noise on the results arises near $Pr = 1$, where very small errors entail big discrepancies in the value of γ, as it is the case for $Pr = 0.71$. As can be seen, if the interpolation of $\overline{\Theta}^+/Pr$ is not done, even higher errors are obtained for γ at Pr near 1, see triangles of Fig. 3b. This is due to the sensitivity of the fitting of an power function near values with base 1. The relation for Δ_θ obtained is $\Delta_\theta = 5.9Pr^{-0.36+0.004Pr}$. The value of γ is reasonable comparable to other values given in previous works, which ranged from -0.3 to -0.5, depending on the Prandtl

Fig. 2. Balances of the (a) moment equation and (b) energy equation for all cases at $Re_\tau = 2000$. Green dashed lines represents the total shear and heat fluxes, blue solid lines are the molecular shear and heat fluxes, black dashed-dotted lines are the turbulent shear and heat fluxes. For both figures, red dotted lines are the differences between the LHS and the RHS of Eqs. (2a) and (2b). Symbols as in Table 1. (For interpretation of the references to color in this figure legend, the reader is referred to the web version of this article.)
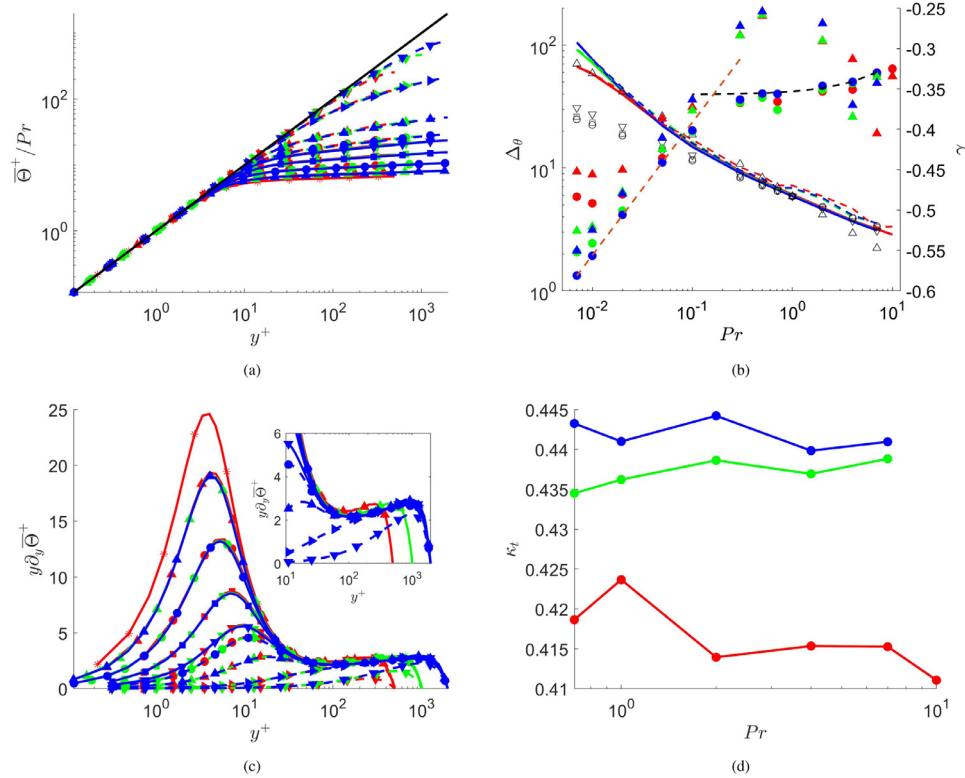
Fig. 3. (a) $\overline{\Theta}^+/Pr$. Black line represents the law of the wall, $\overline{\Theta}^+ = Pr \cdot y^+$. (b) Left axis: solid and dashed lines represent Δ_θ as a function of Pr using and not using a linear interpolation of $\overline{\Theta}^+/Pr$ in between two mesh points, respectively. Black empty symbols represent Δ_θ according to Shaw and Hanratty [27] (squares): $\Delta_\theta \sim Pr^{-0.3}$; Kader [28] (triangle down): $\Delta_\theta \sim Pr^{-1/3}$; Na et al. [6] (triangle up): $\Delta_\theta \sim Pr^{-0.5}$; and Schwertfirm and Manhart [14] (circle): $\Delta_\theta \sim Pr^{-0.29}$. Right axis: circles and triangles represent values of γ with and without the linear interpolation of $\overline{\Theta}^+/Pr$, respectively. Black and orange dashed lines represent the scaling γ for medium–high and low Prandtl numbers, respectively, using the linear interpolation of $\overline{\Theta}^+/Pr$. (d) Diagnosis function of $\overline{\Theta}^+$. Zoom of the logarithmic layer. (f) Von Kármán constant as a function of Prandtl Colours and lines as in Table 1. (For interpretation of the references to color in this figure legend, the reader is referred to the web version of this article.)

number. As seen in Fig. 3b, for high Prandtl numbers, the scaling proposed by Shaw and Hanratty [27] (squares): $\Delta_\theta \sim Pr^{-0.3}$; Kader [28] (triangle down): $\Delta_\theta \sim Pr^{-1/3}$; and Schwertfirm and Manhart [14] (circle): $\Delta_\theta \sim Pr^{-0.29}$, are very precise for the range of Prandtl between 0.3 to 7. Furthermore, the impact on Δ_θ due to the Prandtl number dependence on the exponent appears to be small in the these range of Prandtl numbers. On the other hand, the scaling of Na et al. [6] (triangle up): $\Delta_\theta \sim Pr^{-0.5}$ provides a more precise result for lower Prandtl numbers. Also, remark the small dependence of Pr in the value of γ. Therefore, considering γ constant in a small range of values of Prandtl would not entail big errors. For low Prandtl numbers and sufficiently high Re_τ, the value of γ is a logarithmic function of Pr. The relation in this case is $\Delta_\theta = 5.9Pr^{-0.23+0.071\log(Pr)}$.

As a remark, the definition of Δ_θ could be changed and the limiting value of 5% difference between the wall law and $\overline{\Theta}^+/Pr$ could have been increased or reduced. Then, the value of Δ_θ would had obviously changed. However, in the scaling of Δ_θ with the Prandtl number, the value of γ will remain the same. Therefore, as long as the limiting value of the conductive sublayer is reasonable, the value of γ will always be comparable between different criteria to obtain Δ_θ.

The diagnosis function, β, of the mean temperature is defined as $\beta = y\partial_y\overline{\Theta}^+$. This function is represented in Fig. 3c. If the flow presents a logarithmic layer, then β must be constant in the region approximately between $y^+ = 70$ and $y/h = 0.2$ [29]. In the work done by Jiménez and Moser [30] it was stated that the diagnosis function of the velocity field presents a linear dependence with y^+. This dependence tends to 0 as Re_τ goes to infinity. The same oc-

curs for the diagnosis function of $\overline{\Theta}^+$. This linear dependence with y^+, although small, still exists for $Re_\tau = 2000$. One can see in the zoom of Fig. 3c that in the logarithmic region, where the diagnosis function must be a plateau, there is still a small increment. For cases with the lowest Prandtl numbers, β does not even collapse in the outer region. As the Prandtl number increases, β starts to collapse in the outer region, then in the logarithmic region and for the highest Prandtl numbers, also in the buffer layer. Therefore, for medium–high Prandtl numbers, whether a logarithmic region appears or not for the mean temperature profile will only depend on the Reynolds number.

The previous statement can be confirmed calculating the von Kármán constant, κ_t. It can be obtained by fitting the value of $\overline{\Theta}^+$ in the logarithmic layer to a logarithmic function of the form $\overline{\Theta}^+ = 1/\kappa_t \ln y^+ + B$. The limits of the logarithmic layer where the fitting is done are set to be $y^+ = 70$ for the lower limit and $y/h = 0.2Re_\tau$ for the upper limit, as suggested in [29]. In Fig. 3d, κ_t is represented for the three Reynolds numbers and $Pr \geq 0.71$. It can be seen how κ_t is approximately constant for a constant Re_τ. The small variation (smaller than 2%) can be due to numerical discrepancies. When the Reynolds number is increased, κ_t slightly increases. Also, differences of κ_t were expected, since for these values of Reynolds number, the logarithmic layer is not perfectly developed. Nevertheless, the value of κ_t seems to converge with the Reynolds number towards a value of roughly 0.45 or slightly above. This result is very close to to the one provided in the work of Pirozzoli et al. [10], where a value of $\kappa_t = 0.46$ is obtained for $Re_\tau = 4000$ and a thermal boundary condition that consisted in a thermal heat generation. Regarding the work of Abe and Antonia
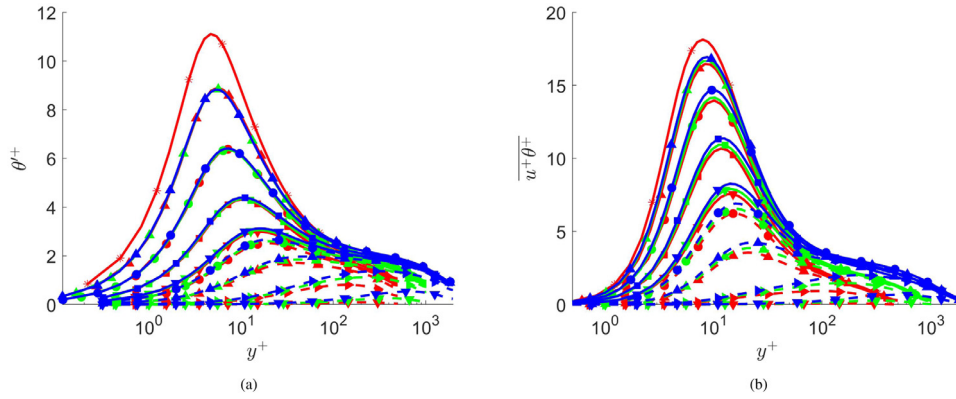
Fig. 4. (a) Temperature fluctuation, θ'^+ and (b) streamwise heat flux, $\overline{u^+\theta^+}$. Colours and lines as in Table 1.

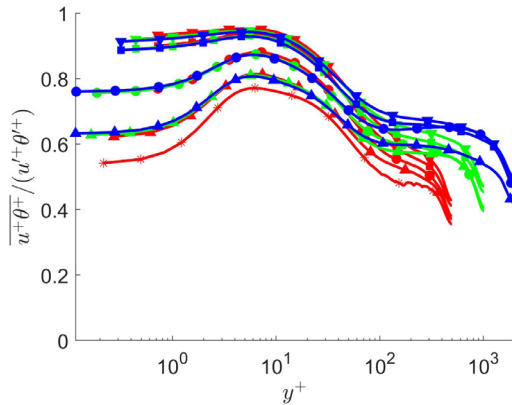Fig. 5. Correlation coefficient between $\overline{u^+\theta^+}/(u'^+\theta'^+)$. Colours and lines as in Table 1.

[31], where the MBC was also used, a value of $\kappa_t = 0.43$ was obtained for $Re_\tau = 1000$, which agrees with the one presented in this work.

Turbulent intensities such as the transformed temperature fluctuation, θ'^+, the streamwise heat flux, $\overline{u^+\theta^+}$ and the wall-normal heat flux, $\overline{v^+\theta^+}$ have been calculated. They are represented in Figs. 4, 5 and 6 a, as a function of the inner coordinates. One of the main differences between θ'^+ and $\overline{u^+\theta^+}$, is that, at the highest Prandtl numbers, or more precisely, highest friction Péclet numbers, $Pe_\tau = Re_\tau Pr$, the maximum of θ'^+ does not grow with the Reynolds number (see Fig. 4a). Analogously, this feature is observed in Couette flows for the velocity fluctuation, u'^+, when the Reynolds number is high enough [32]. However, up to the knowledge of the authors, this is the first time that this feature is reported for a thermal Poiseuille flow. This scaling of the maximum of θ'^+ have more benefits in the scaling of some turbulent budgets, as will be seen in the next subsection.

It was shown before that, near the wall, the streamwise velocity and the temperature field are highly correlated (Fig. 1f), specially for Prandtl numbers close to 1. But it was mentioned that, as the Prandtl number moves away from 1 this correlation is weaker. In Fig. 5, the correlation coefficient is shown for all cases with $Pr \geq 1$. The same tendencies were obtained by Abe et al. [17] for cases with lower Reynolds numbers and Prandtl close to 1. Note that some noise appears at the center due to small values of $\overline{u^+\theta^+}$, u'^+ and θ'^+. Nevertheless, the important result is obtained at $y^+ \approx 10$, where, effectively, the correlation coefficient decreases from 0.95 for $Pr = 1$, down to 0.8 for $Pr = 7$.

Finally, $\overline{v^+\theta^+}$ represents the turbulent heat flux. For higher Pe_τ, $\overline{v^+\theta^+}$ approaches to its bound value of -1 in a wider region of

y (see Fig. 6a). This is in accordance with Townsend's hypothesis [33], applied to the temperature field. Additionally, a quadrant analysis like in [34] has been performed to study the generation mechanism of $\overline{v^+\theta^+}$ compared with the one of $\overline{u^+v^+}$ (Fig. 6b, c and d). On one hand, events on the first quadrant, Q1 (θ, $u > 0$ and $v > 0$), and third quadrant, Q3 (θ, $u < 0$ and $v < 0$), are referred to as outward and inward interactions, respectively. On the other hand, the second quadrant, Q2 (θ, $u < 0$ and $v > 0$), and fourth quadrant, (θ, $u > 0$ and $v < 0$), represent ejection and sweep events, respectively. A good scaling in the Reynolds number is observed from Fig. 6c and d, with indeed similar tendencies for both $\overline{v^+\theta^+}$ and $\overline{u^+v^+}$. Dominant contributions from the sweep events (Q4) appear very close to the wall. At a certain y^+ coordinate, the ejection events (Q2) become the most important. Obviously, this y^+ coordinate is constant for different Reynolds numbers, since the generation mechanism scales with Re_τ. However, the y^+ coordinate where the alternation of the dominant event occurs moves closer to the wall as the Prandtl number increases, going from $y^+ = 16$ for $Pr = 1$ (similar to the $y^+ = 17$ for $Pr = 0.71$ obtained in [34]) to $y^+ = 8$ for $Pr = 7$ (see Fig. 6b). Related with the constant maximum of θ'^+ for different Reynolds numbers, one can see how the maximums of Q1, Q2 and Q3 events also scale for $\overline{v^+\theta^+}$, in contrast to $\overline{u^+v^+}$, where all maximums increase with the Reynolds number, as in $\overline{u^+\theta^+}$. Regarding the scaling in the outer region, a good similarity is observed for the cases at $Re_\tau = 2000$ and $Pr = 4$ and 7 in Fig. 6b. However, if the Reynolds or Prandtl number are decreased, some discrepancies appear, specially in the region below $y/h < 0.3$ (see Fig. 6c. The same result was obtained by Abe and Antonia [34] for a low Prandtl number of 0.025 and Reynolds number ranging from 180 up to 1020.

Two important dimensionless numbers, such as the Nusselt number, Nu, and the turbulent Prandtl number, Pr_t, have been calculated. Their definitions are

$$Nu = \frac{L\mathfrak{h}}{\kappa} = \frac{2Re_\tau Pr}{\langle \overline{\Theta}_m^+ \rangle}; \quad \text{where} \quad \langle \overline{\Theta}_m^+ \rangle = \frac{\int_0^1 \overline{U}^+ \overline{\Theta}^+ dy^*}{\int_0^1 \overline{U}^+ dy^*}, \quad (3a)$$

$$Pr_t = \frac{\nu_t}{\kappa_t} = \frac{\overline{u^+v^+}}{\overline{v^+\theta^+}} \frac{d\overline{\Theta}^+/dy^+}{d\overline{U}^+/dy^+}. \quad (3b)$$

In Fig. 7, Nu is presented as a function of Pr. It was shown in [12] that Nu is a power function of Pr for $Pe \leq 20$. Also, in [5], it was noted that, for $Re_\tau = 180$, the increment of Nu begins to reduce for Prandtl numbers greater than 1. This feature is also observed here for medium–high Prandtl numbers at Re_τ up to 2000. However, it is not Pr that determines when Nu is no longer a power function of Pr, but Pe_τ. As a conclusion, Nu is a power function of Pr in the specific range of the friction Péclet number,
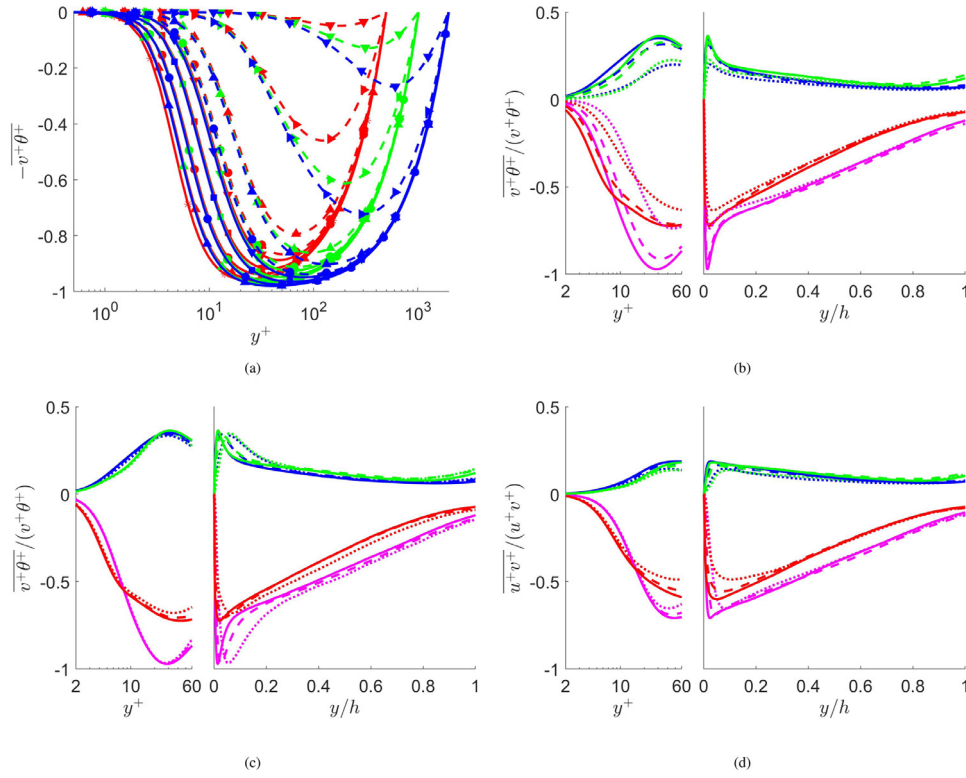
Fig. 6. (a) wall-normal heat flux, $\overline{v^+\theta^+}$. Quadrant analysis of $\overline{v^+\theta^+}$ for (b) $Re_\tau = 2000$ and different Prandtl numbers: $Pr = 1$ (dotted lines), $Pr = 4$ (dashed lines) and $Pr = 7$ (solid lines) and (c) $Pr = 7$ and different Reynolds numbers: $Re_\tau = 500$ (dotted lines), $Re_\tau = 1000$ (dashed lines) and $Re_\tau = 2000$ (solid lines). (d) Quadrant analysis of $\overline{u^+v^+}$ for $Pr = 7$ and different Reynolds numbers: $Re_\tau = 500$ (dotted lines), $Re_\tau = 1000$ (dashed lines) and $Re_\tau = 2000$ (solid lines). In (b), (c) and (d) colour blue is for events of Q1, magenta for Q2, green for Q3 and red for Q4. (For interpretation of the references to color in this figure legend, the reader is referred to the web version of this article.)
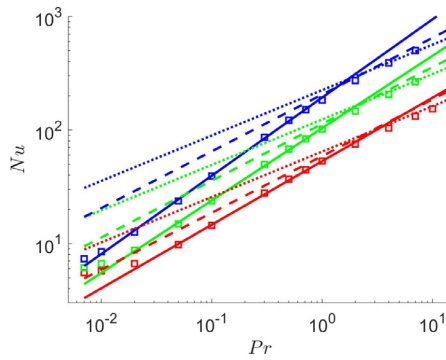

Fig. 7. Nu as a function of Pr. Squares are the values from the DNS. Solid lines represent correlations from this work (4a)–(4c). Dotted lines represent Dittus and Boelter correlation (5) Finally, dashed lines represent Kays et al. correlation (6). Colours and lines as in Table 1.

$20 \leq Pe_\tau \leq 1500$

$$Nu = 53.1Pr^{0.560}, \text{ for } Re_\tau = 500 \tag{4a}$$

$$Nu = 103.7Pr^{0.638}, \text{ for } Re_\tau = 1000 \tag{4b}$$

$$Nu = 192.9Pr^{0.689}, \text{ for } Re_\tau = 2000 \tag{4c}$$

for $20 \leq Pe_\tau \leq 1500$. Two more correlations are also included in Fig. 7. On one hand, the correlation obtained by Dittus and Boelter [35] for turbulent pipe flows

$$Nu = 0.023Re_D^{0.8}Pr^n, \tag{5}$$

where Re_D is the Reynolds number based on the diameter of the pipe and $n = 0.4$ since the flow is being heated. On the other hand,

the correlation obtained by Kays et al. [36] for constant temperature walls, which reads

$$Nu = 0.021Re^{0.8}Pr^{0.5} \tag{6}$$

The correlation proposed in the work (4c) is very precise in the range of $20 \leq Pe_\tau \leq 1500$. However, as mention before, for Prandtl numbers above 1 the scaling of Nu with Pr changes and, in the small range obtained here, Dittus and Boelter correlation (5) fits well with an exponent of 0.4 in the Prandtl, while the exponent of 0.5 from the Kays et al. correlation (6) seems to be overestimating the value of Nu. Nevertheless, if the scaling of Nu for higher Prandtl numbers is still a power function of Pr with exponent approximately 0.4 can not be determined with the data from this work only. Higher Prandtl numbers must be simulated. This, however, is beyond the scope of the study of this work.

With respect to Pr_t an important change in its value near the wall occurs (Fig. 8a). For medium molecular Prandtl numbers, Pr_t value is approximately 1.1 at the wall, as reported by many other authors [4,5,34,37,38]. However, for medium–high Prandtl numbers, Pr_t in the wall increases. The reason of this increase can be explained through a decomposition of the fluctuating variables near the wall [5]

$$\theta'^+ = Pr\left(a_\theta y^+ + \mathcal{O}(y^{+2})\right), \tag{7a}$$

$$\overline{u^+\theta^+} = Pr\left(b_{1\theta}y^{+2} + \mathcal{O}(y^{+3})\right), \tag{7b}$$

$$\overline{v^+\theta^+} = Pr\left(c_{2\theta}y^{+3} + \mathcal{O}(y^{+4})\right), \tag{7c}$$

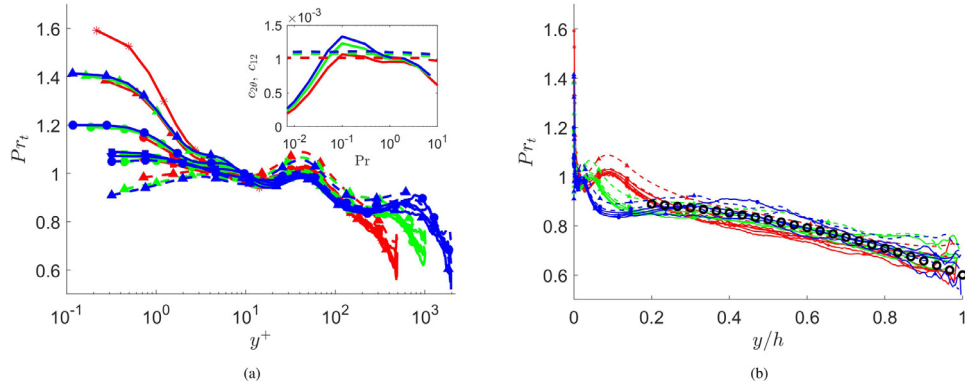$$\overline{u^+v^+} = c_{12}y^{+3} + \mathcal{O}(y^{+4}). \tag{7d}$$

Fig. 8. (a) Pr_t focused in the near-wall region. Box: Values of $c_{2\theta}$ (solid) and c_{12} (dashed). (b) Pr_t in the core region. Black circles represent the distribution proposed by Abe and Antonia [17]. Colours and lines as in Table 1.

Using the definition of Pr_t, (3b), where $(d\overline{\Theta}^+/dy^+)/(d\overline{U}^+/dy^+) = Pr$ at the wall, and the approximations of $\overline{v^+\theta^+}$ and $\overline{u^+v^+}$ near the wall, (7c) and (7d), respectively, one gets $Pr_t|_{y=0} \approx c_{12}/c_{2\theta}$.

The value of these coefficients can be observed in the box inside Fig. 8a. The coefficient $c_{2\theta}$ has a constant value approximately equal to c_{12} in the range of Prandtl numbers near one. However, for $Pr \geq 4$, $c_{2\theta}$ decreases due to the reduction of the normal-wall heat fluxes over the Prandtl number, i.e. $\overline{v^+\theta^+}/Pr$ reduces when the Prandtl is increased above $Pr \approx 4$. This makes Pr_t greater than 1 in the wall. This variation has serious consequences in the modelling of fluids with medium–high Prandtl number, like water, since Pr_t is one the the main parameters for modelling.

In the core region of the channel, Abe and Antonia [17] proposed a quadratic distribution for Pr_t

$$Pr_t = 0.9 - 0.3(y/h)^2. \tag{8}$$

In Fig. 8b, it is observed how this approximation captures the mean behaviour of Pr_t, even for Reynolds and Prandtl numbers up to 2000 and 7, respectively.

3.2. Turbulent budgets

Turbulent budgets of the temperature variance, $k_\theta = (1/2)\overline{\theta^2}$, the dissipation rate of the temperature variance, ε_θ, and the streamwise, $\overline{u\theta}$, and wall-normal heat flux, $\overline{v\theta}$, are analyzed in this subsection. The transport equations that define each budget term can be obtained from the governing equations. In the case of k_θ, it reads

$$\frac{Dk_\theta}{Dt} = P + T + V + \varepsilon_\theta, \tag{9}$$

where D/Dt is the mean substantial derivative and each term on the right hand side represent the production, turbulent diffusion, viscous diffusion and dissipation of the temperature variance. These four terms are defined as

$$P = -\overline{v\theta}\,\partial_y\overline{\Theta}, \tag{10a}$$

$$T = -\frac{1}{2}\partial_y\overline{\theta^2 v}, \tag{10b}$$

$$V = \frac{1}{2Pr}\partial_{yy}^2\overline{\theta^2}, \tag{10c}$$

$$\varepsilon_\theta = -\frac{1}{Pr}\overline{\partial_i\theta\,\partial_i\theta}. \tag{10d}$$

The transport equation for ε_θ can be written as

$$\frac{D\varepsilon_\theta}{Dt} = P_m + P_{mg} + P_g + P_t + T_t + V_{\varepsilon_\theta} + \varepsilon_{\theta 1}. \tag{11}$$

Here, four production terms arise. From left to right on Eq. (11) these production terms are named mixed production, mean gradient production, gradient production and turbulent production. The last three terms are the turbulent diffusion, molecular diffusion and dissipation of the dissipation rate of the temperature variance. Each term is defined as

$$P_m = -\frac{2}{Pr}\overline{\partial_i v\,\partial_i\theta}\,\partial_y\overline{\Theta}, \tag{12a}$$

$$P_{mg} = -\frac{2}{Pr}\overline{\partial_x\theta\,\partial_y\theta}\,\partial_y\overline{U}, \tag{12b}$$

$$P_g = -\frac{2}{Pr}\overline{v\,\partial_y\theta}\,\partial_{yy}^2\overline{\Theta}, \tag{12c}$$

$$P_t = -\frac{2}{Pr}\overline{\partial_i\theta\,\partial_j\theta\,\partial_j u_i}, \tag{12d}$$

$$T_t = -\frac{1}{Pr}\partial_y\overline{v\,\partial_i\theta\,\partial_i\theta}, \tag{12e}$$

$$V_{\varepsilon_\theta} = \frac{1}{Pr^2}\partial_{yy}^2\varepsilon_0, \tag{12f}$$

$$\varepsilon_{\theta 1} = -\frac{2}{Pr^2}\overline{\partial_{kj}^2\theta\,\partial_{kj}^2\theta}. \tag{12g}$$

Finally, the transport equation of $\overline{u_i\theta}$ can be written as

$$\frac{D\overline{u_i\theta}}{Dt} = P_i + T_i + V_i + \varepsilon_i + \Pi_i^s + \Pi_i^d. \tag{13}$$

The previous four budget terms appear, namely production, turbulent diffusion, viscous diffusion and dissipation of the heat fluxes. In addition, two extra terms related with pressure appear in the transport equation: pressure-temperature gradient correlation and pressure diffusion. They are respectively defined as

$$P_i = -\overline{u_i v}\,\partial_y\overline{\Theta} - \overline{v\theta}\,\partial_y\overline{U_i}, \tag{14a}$$

$$T_i = -\partial_{x_k}\overline{u_i u_k\theta}, \tag{14b}$$

$$V_i = \nu\partial_{x_k}\left(\overline{\theta\,\partial_{x_k}u_i} + \frac{1}{Pr}\overline{u_i\,\partial_{x_k}\theta}\right), \tag{14c}$$

$$\Pi_i^s = \overline{p\,\partial_{x_i}\theta}, \tag{14d}$$

$$\Pi_i^d = -\partial_{x_k}\left(\delta_{ki}\overline{p\theta}\right), \tag{14e}$$

$$\varepsilon_i = -\nu\left(1 + \frac{1}{Pr}\right)\overline{\partial_{x_k}u_i\,\partial_{x_k}\theta}, \tag{14f}$$
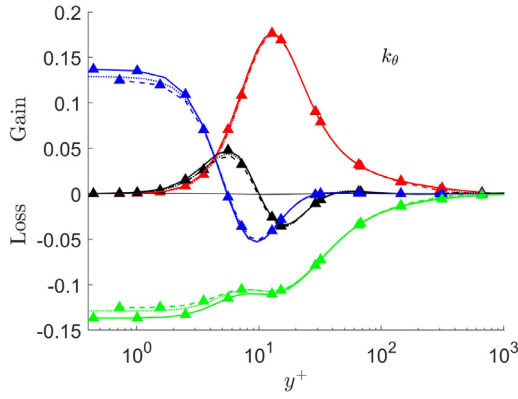
Fig. 9. Budgets of the temperature variance, k_θ for $Pr = 0.71$. Here, colours denote budget terms: production, turbulent diffusion (black), viscous diffusion (blue) and dissipation (green). Here, line style denotes the Reynolds number: $Re_\tau = 2000$ in solid lines and $Re_\tau = 500$ in dashed lines are from [12], where the same code that in this work was used. $Re_\tau = 640$ in dotted lines is from Abe et al. [8]. (For interpretation of the references to color in this figure legend, the reader is referred to the web version of this article.)

where δ_{ij} is Kronecker's delta and repeated index imply summation over $k = 1, 2, 3$.

Although it was stated in section §2 that the size of the computational box, $L_x = 2\pi h$, $L_y = 2h$ and $L_z = \pi h$, was enough to accurately compute first order statistics, it is also big enough to calculate the turbulent budgets. Fig. 9 presents the budget terms of k_θ obtained by the code used in this work, for $Pr = 0.71$ and $Re_\tau = 500$ (dashed lines) and 1000 (solid lines). These results have been compared with those obtained by Abe et al. [8] for $Pr = 0.71$ and $Re_\tau = 640$ (dotted lines). The size of the computational box used by Abe et al. [8] is $L_x = 4\pi h$, $L_y = 2h$ and $L_z = 2\pi h$. A perfect collapsing or following of the trends is observed for the budgets

of k_θ. The same results have been obtained for the budget terms of the heat fluxes, but they are not shown here for brevity. This validates the size of the computational box used in this work to calculate turbulent budgets.

Fig. 10 a, b, c and d present the results obtained for every budget term of Eqs. (9)–(14). Only simulations for the three Reynolds numbers, $Re_\tau = 500$, 1000 and 2000, with $Pr = 2$ and 7 are plotted. The main result obtained is the better scaling near the wall of the viscous diffusion, V, and the dissipation, ε_θ, in the budget of k_θ. For $Pr = 7$, V^+ varies less than 5% in the wall between cases $Re_\tau = 500$ and 2000. This is a significant reduction compared with the 16% difference obtained for $Pr = 0.71$ [12].

The value of V^+ and ε_θ^+ at the wall can be calculated as

$$ V^+\big|_{y\to 0} = \frac{1}{2Pr}\partial_{yy}\overline{\theta'^{+2}}\bigg|_{y\to 0} = -\varepsilon_\theta^+\big|_{y\to 0}. \tag{15} $$

Using the approximation of θ'^+ near the wall from Eq. (7a), one gets

$$ V^+\big|_{y\to 0} = -\varepsilon_\theta^+\big|_{y\to 0} \approx Pr \cdot a_\theta^2. \tag{16} $$

If the first maximum of θ^+ is constant and it is placed at the same distance to the wall, a_θ will be the same for two cases with the same Prandtl. It was shown before (Fig. 4a), that this is fulfilled for medium–high Prandtl numbers. Therefore, since a_θ is approximately constant, a good scaling is obtained in the wall. Note that the scaling of $V^+\big|_{y\to 0}$ and $\varepsilon_\theta^+\big|_{y\to 0}$ with a_θ is quadratic, so small differences in a_θ will make scaling errors larger. In Fig. 11a the values of a_θ for all simulations are represented (solid lines and left axis). Effectively, when the Prandtl number is increased, the values of a_θ converge among the three different Reynolds numbers. Furthermore, a_θ seems to converge to a value between 0.3 and 0.4.

In the ideal case where a_θ does not depend neither on Re_τ nor Pr, V/Pr and ε_θ/Pr will perfectly scale in the wall for all Re_τ and Pr. If, in addition, the wall-normal direction is scaled with $Pr^{1/3}$, as in
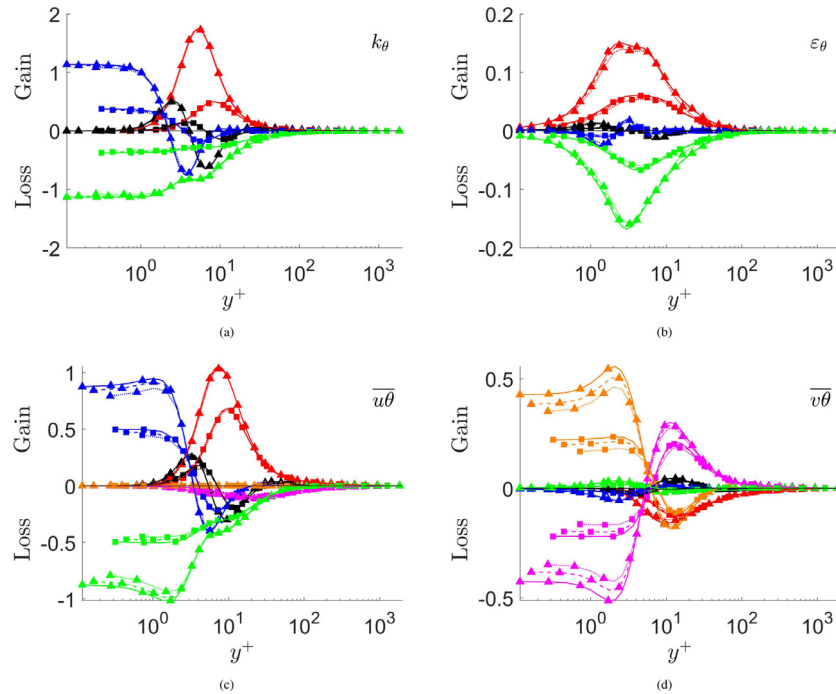

Fig. 10. Budgets of (a) temperature variance, k_θ, (b) dissipation rate of the temperature variance, ε_θ, (c) streamwise heat flux, $\overline{u\theta}$, and (d) wall-normal heat flux, $\overline{v\theta}$. Here, colours denote budget terms: production or sum of productions in (b) (red), turbulent diffusion (black), viscous diffusion (blue), dissipation (green), pressure strain (magenta) and pressure diffusion (orange). Here, line style denotes the Reynolds number: $Re_\tau = 2000$ in solid lines, $Re_\tau = 1000$ in dashed lines and $Re_\tau = 500$ in dotted lines. Black line with value 0 is the summation of all terms. Symbols as in Table 1. (For interpretation of the references to color in this figure legend, the reader is referred to the web version of this article.)
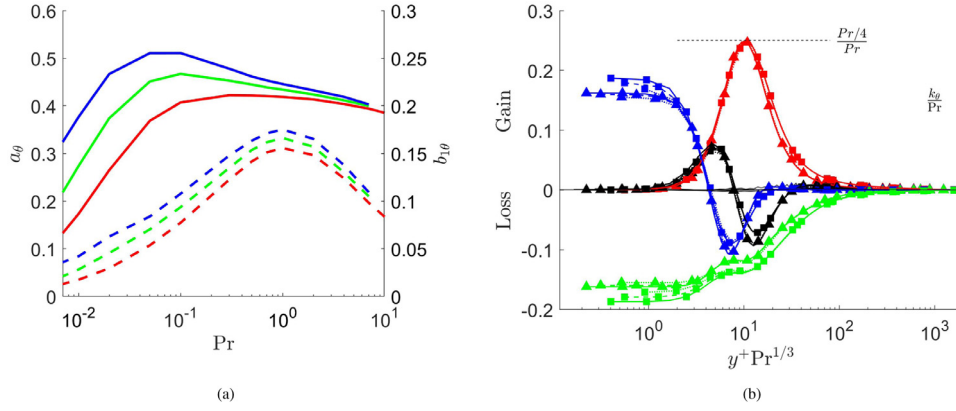
Fig. 11. (a) Values of a_θ (solid and left axis) and $b_{1\theta}$ (dashed and right axis). Colours as in Table 1. (b) Budgets of k_θ/Pr as a function of $y^+Pr^{1/3}$. Cases for $Pr = 4$ and 7 are represented. Here, colours denote budget terms: production (red), turbulent diffusion (black), viscous diffusion (blue) and dissipation (green). Here, line style denotes the Reynolds number: $Re_\tau = 2000$ in solid lines, $Re_\tau = 1000$ in dashed lines and $Re_\tau = 500$ in dotted lines. Black line with value 0 is the summation of all terms. Symbols as in Table 1. (For interpretation of the references to color in this figure legend, the reader is referred to the web version of this article.)
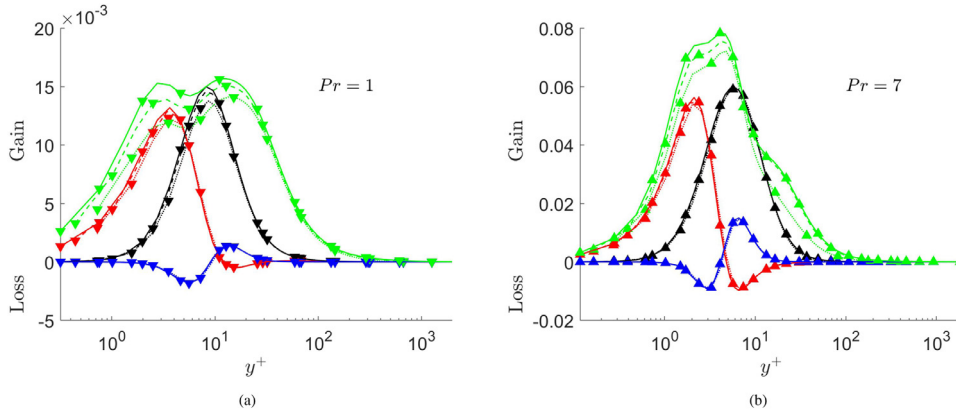

Fig. 12. Production terms of ε_θ. (a) $Pr = 1$ and (b) $Pr = 7$. Here, colours denote production term: mixed production (red), mean gradient production (black), gradient production (blue) and turbulent production (green). Here, line style denotes the Reynolds number: $Re_\tau = 2000$ in solid lines, $Re_\tau = 1000$ in dashed lines and $Re_\tau = 500$ in dotted lines. Symbols as in Table 1. (For interpretation of the references to color in this figure legend, the reader is referred to the web version of this article.)

[5], the peaks of the other terms will also scale. The results for the cases of $Pr = 2$ and 7 are shown in Fig. 11b. The scaling is almost perfect in the entire channel except in the wall, where the small differences in a_θ are amplified due to this quadratic behaviour. In this context, Abe and Antonia [31] found that the peak value of the product term reaches a constant maximum of value $Pr/4$ for the thermal boundary condition used in this work, MBC, for Re_τ larger than 400. This seems to be convincing with the result obtained for Re_τ up to 2000.

Following this procedure, the same analysis can be done for the viscous diffusion, V_u, and dissipation, ε_u, in the budget of $\overline{u\theta}$. Their values at the wall are obtained using (7b)

$$V_u^+\big|_{y\to 0} = -\varepsilon_u^+\big|_{y\to 0} \approx \frac{Pr+1}{Pr}\partial_{yy}\overline{u^+\theta^+}\big|_{y\to 0} = (Pr+1)b_{1\theta}. \quad (17)$$

Therefore, if the $b_{1\theta}$ values are different, V_u and ε_u will not scale in the wall. In Fig. 11a, the values of $b_{1\theta}$ are represented with dashed lines (right axis). Effectively, $b_{1\theta}$ is not the same for different Reynolds numbers. In addition, $b_{1\theta}$ oscillates for different Prandtl numbers.

Finally, regarding the budgets of ε_θ, Abe et al. [17] did an analysis focusing of the Reynolds dependence of the production terms of the transport equation of the mean square scalar gradient, whose terms are analogous to the ones of ε_θ, defined in Eq. (12). They found that for $Pr = 0.71$, with the increase of the

friction Reynolds number, from $Re_\tau = 180$ up to 640, the mixed production, mean gradient production and turbulent production also increased. Meanwhile, the gradient production term was independent of the Reynolds number. The same tendency can be observed in Fig. 12a, where the product terms of ε_θ are shown for $Pr = 1$ up to $Re_\tau = 2000$. However, an interesting result is obtained when the Prandtl number is increased to $Pr = 7$ (Fig. 12b). At this higher Prandtl number, the mixed and mean gradient production seem to be independent of the Reynolds number when this is high enough, i.e. $Re_\tau \geq 1000$. Therefore, the only Reynolds dependent term is the turbulent production. Although not shown here for the sake of brevity, for $Pr = 4$ a clearer difference was notice between the mixed and mean gradient production terms at $Re_\tau = 500$ and 1000. This suggests that a thermal equilibrium is achieved depending on a combination of Re_τ and Pr, i.e. the Péclet number, Pe_τ. This thermal equilibrium may be linked with the inner collapsing obtained for the thermal fluctuations with high Péclet numbers (Fig. 4a).

4. Conclusions

A new set of DNS in a thermal channel flow at medium and medium–high Prandtl numbers has been conducted. The MBC has been used as the thermal boundary condition. The mean temperature field has been studied and a new scaling for the thick-

ness of the conductive sublayer has been proposed for medium to medium–high Prandtl numbers, $\Delta_\theta \sim Pr^{-0.36+0.004Pr}$.

The presence of a logarithmic region in the temperature field is still not perfectly observed at the ranges of Re_τ and Pr simulated, although the Reynolds number dependencies are small. Also, it is demonstrated that, for medium and medium–high Prandtl numbers, whether or not the logarithmic layer perfectly appears, depends only on the Reynolds number. Therefore, the values of κ_t are constant for different Prandtl number, but converges towards a constant value when the Reynolds number tends to infinity.

Turbulent intensities have been calculated. The main result is that for the first time, it is observed in thermal channel flows, that the maximum value of θ' does not increase when Re_τ is increased for medium–high Prandtl numbers. As a consequence, in the budgets of the temperature variance, the scaling of the viscous diffusion and dissipation terms is more accurate near the wall. This may also be the consequence of a Reynolds number independence of the mixed and mean gradient production terms in the transport equation of ε_θ. As a conclusion, a thermal equilibrium seems to be achieved in the near-wall region when the Pe_τ number is high enough, so that the aforementioned thermal quantities become constant with the Reynolds number.

Finally, the Nusselt and the turbulent Prandtl numbers have been calculated. It is observed how the Nu can be written as a power function of Pr in a range of Pe_τ between 20 and 1500. On the other hand, Pr_t is no longer equal to 1 near the wall for medium–high Prandtl numbers. Pr_t increases due to the decrease of the wall-normal heat flux near the wall, which entails a lower thermal eddy diffusivity.

Remark, that the Prandtl numbers simulated in this work reach up to the Prandtl number of water ($Pr \approx 7$), and with the Reynolds numbers reached, up to $Re_\tau = 2000$, these new features of the thermal field have been obtained. The tendency has been to observe statistics that become Reynolds independent when the Reynolds was increased (θ'^+, the viscous diffusion and dissipation budgets of k_θ near the wall, and the mixed and mean gradient production budget terms of ε_θ). Although an extrapolation should always be made carefully, the Reynolds numbers in practical applications are even well above $Re_\tau = 2000$, which suggest that a perfect scaling with Re_τ is achieved for this variables, making thermal models for water much easier and accurate.

The raw data that support the findings of this study are available from the corresponding author upon reasonable request. One point statistics can be downloaded from the web page of our group: http://personales.upv.es/serhocal/.

Credit Author Statement

Both authors, Francisco Alcántara-Ávila and Sergio Hoyas, have contributed in the same way in the elaboration of the article.

Declaration of Competing Interest

The authors declare that they have no known competing financial interests or personal relationships that could have appeared to influence the work reported in this paper.

Acknowledgments

References

[1] J. Kim, P. Moin, R. Moser, Turbulence statistics in fully developed channels flows at low Reynolds numbers, J. Fluid Mech. 177 (1987) 133–166.

[2] J. Kim, P. Moin, Transport of passive scalars in a turbulent channel flow, NASA 1 (TM-89463) (1987) 1–14.

[3] S. Lyons, T. Hanratty, J. McLaughlin, Direct numerical simulation of passive heat transfer in a turbulent channel flow, Int. J. Heat Mass Transf. 34 (4-5) (1991) 1149–1161, doi:10.1016/0017-9310(91)90024-9.

[4] N. Kasagi, Y. Tomita, A. Kuroda, Direct numerical simulation of passive scalar field in a turbulent channel flow, J. Heat Transf. 114 (3) (1992) 598–606.

[5] H. Kawamura, K. Ohsaka, H. Abe, K. Yamamoto, DNS of turbulent heat transfer in channel flow with low to medium-high Prandtl number fluid, Int. J. Heat Fluid Flow 19 (5) (1998) 482–491.

[6] Y. Na, D. Papavassiliou, T. Hanratty, Use of direct numerical simulation to study the effect of Prandtl number on temperature fields, Int. J. Heat Fluid Flow 20 (3) (1999) 187–195.

[7] H. Kawamura, H. Abe, K. Shingai, DNS of turbulence and heat transport in a channel flow with different Reynolds and Prandtl numbers and boundary conditions, in: Turbulence, Heat and Mass Transfer 3 (Proc. of the 3rd International Symposium on Turbulence, Heat and Mass Transfer), 2000.

[8] H. Abe, H. Kawamura, Y. Matsuo, Surface heat-flux fluctuations in a turbulent channel flow up to $Re_\tau = 1020$ with $Pr = 0.025$ and 0.71, Int. J. Heat Fluid Flow 25 (3) (2004) 404–419.

[9] M. Kozuka, Y. Seki, H. Kawamura, DNS of turbulent heat transfer in a channel flow with a high spatial resolution, Int. J. Heat Fluid Flow 30 (3) (2009) 514–524.

[10] S. Pirozzoli, M. Bernardini, P. Orlandi, Passive scalars in turbulent channel flow at high Reynolds numbers, J. Fluid Mech. 788 (2016) 614–639.

[11] F. Lluesma-Rodríguez, S. Hoyas, M. Peréz-Quiles, Influence of the computational domain on DNS of turbulent heat transfer up to $Re_\tau = 2000$ for $Pr = 0.71$, Int. J. Heat Mass Transf. 122 (2018) 983–992.

[12] F. Alcántara-Ávila, S. Hoyas, M. Pérez-Quiles, DNS of thermal channel flow up to $Re_\tau = 2000$ for medium to low Prandtl numbers, Int. J. Heat Mass Transf. 127 (2018) 349–361, doi:10.1016/j.ijheatmasstransfer.2018.06.149.

[13] Y. Seki, K. Iwamoto, H. Kawamura, Prandtl number effect on turbulence quantities through high spatial resolution DNS of turbulent heat transfer in a channel flow, in: Dubrovnik, Croatia, Ch. Fifth Int. Symp. on Turbulence, Heat and Mass Transfer, 2006, pp. 301–304.

[14] F. Schwertfirm, M. Manhart, DNS of passive scalar transport in turbulent channel flow at high Schmidt numbers, Int. J. Heat Fluid Flow 28 (6) (2007) 1204–1214.

[15] T. Yano, N. Kasagi, Direct numerical simulation of turbulent heat transport at high Prandtl numbers, JSME Int. J. Ser. B 42 (2) (1999) 284–292.

[16] H. Kawamura, H. Abe, Y. Matsuo, DNS of turbulent heat transfer in channel flow with respect to Reynolds and Prandtl number effects, Int. J. Heat Fluid Flow 20 (1999) 196–207.

[17] H. Abe, R.A. Antonia, H. Kawamura, Correlation between small-scale velocity and scalar fluctuations in a turbulent channel flow, J. Fluid Mech. 627 (2009) 1–32.

[18] A. Lozano-Durán, J. Jiménez, Effect of the computational domain on direct simulations of turbulent channels up to $Re_\tau = 4200$, Phys. Fluids 26 (1) (2014) 011702, doi:10.1063/1.4862918.

[19] S. Hoyas, J. Jiménez, Scaling of the velocity fluctuations in turbulent channels up to $Re_\tau = 2003$, Phys. Fluids 18 (1) (2006) 011702.

[20] S. Hoyas, J. Jiménez, Reynolds number effects on the Reynolds-stress budgets in turbulent channels, Phys. Fluids 20 (10) (2008) 101511.

[21] V. Avsarkisov, S. Hoyas, M. Oberlack, J. García-Galache, Turbulent plane Couette flow at moderately high Reynolds number, J. Fluid Mech. 751 (2014) R1.

[22] S. Gandía-Barberá, S. Hoyas, M. Oberlack, S. Kraheberger, The link between the Reynolds shear stress and the large structures of turbulent Couette-Poiseuille flow, Phys. Fluids 30 (4) (2018) 041702, doi:10.1063/1.5028324.

[23] F. Alcántara-Ávila, G. Barberá, S. Hoyas, Evidences of persisting thermal structures in Couette flows, Int. J. Heat Fluid Flow 76 (2019) 287–295, doi:10.1016/j.ijheatmasstransfer.2018.06.149.

[24] S.K. Lele, Compact finite difference schemes with spectral-like resolution, J. Comput. Phys. 103 (1) (1992) 16–42.

[25] P.R. Spalart, R.D. Moser, M.M. Rogers, Spectral methods for the Navier-Stokes equations with one infinite and two periodic directions, J. Comput. Phys. 96 (2) (1991) 297–324.

[26] S. Pirozzoli, M. Bernardini, P. Orlandi, Turbulence statistics in Couette flow at high Reynolds number, J. Fluid Mech. 758 (2014) 323–343, doi:10.1017/jfm.2014.529.327.

[27] D. Shaw, T. Hanratty, Turbulent mass transfer rates to a wall for large schmidt numbers, AIChE J. 23 (1) (1977) 28–37, doi:10.1002/aic.690230106.

[28] B. Kader, Temperature and concentration profiles in fully turbulent boundary layers, Int. J. Heat Mass Transf. 24 (9) (1981) 1541–15441.

[29] J. Jiménez, Near-wall turbulence, Phys. Fluids 25 (10) (2013) 101302.

[30] J. Jiménez, R.D. Moser, What are we learning from simulating wall turbulence? Phil. Trans. R. Soc. Lond. A 365 (2007) 715–732.

[31] H. Abe, R.A. Antonia, Relationship between the heat transfer law and the scalar dissipation function in a turbulent channel flow, J. Fluid Mech. 830 (2017) 300–325.

[32] S. Hoyas, K. Stefanie, M. Oberlack, F. Alcántara-Ávila, Turbulent Couette flow up to $Re_\tau = 2000$ – a DNS study and symmetry induced scaling laws, TBC ? (2020).

[33] A. Townsend, The Structure of Turbulent Shear Flows, second ed., Cambridge University Press, New York,, 1976.

[34] H. Abe, R.A. Antonia, Mean temperature calculations in a turbulent channel flow for air and mercury, Int. J. Heat Mass Transf. 132 (2019) 1152–1165.

[35] F.W. Dittus, L.M.K. Boelter, Heat transfer in automobile radiators of the tubular type, Publ. Eng. 2 (13) (1930) 443–461.

[36] W.M. Kays, M. Crawford, B. Weigand, Convective Heat and Mass Transfer, Mc-Graw-Hill (1980).

[37] R.A. Antonia, K. J., Turbulent Prandtl number in the near-wall region of a turbulent channel flow, Int. J. Heat Mass Transf. 34 (7) (1991) 1905–1908.

[38] Y. Na, T. Hanratty, Limiting behavior of turbulent scalar transport close to a wall, Int. J. Heat Mass Transf. 43 (10) (2000) 1749–1758.